Journal of Food Composition and Analysis 135 (2024) 106667

Contents lists available at ScienceDirect

Journal of Food Composition and Analysis

journal homepage: www.elsevier.com/locate/jfca

# A versatile pH-sensitive hydrogel based on a high-performance dye: Monitoring the freshness of milk and chicken meat

Rosita Diana [a,*], Ludovica Milzi [a], Francesco Silvio Gentile [b], Marianna Pannico [c], Pellegrino Musto [c], Anna Maiello [d], Barbara Panunzi [a]

[a] Department of Agriculture, University of Napoli Federico II, Via Università, 100, Portici, NA 80055, Italy
[b] Department of Chemical Sciences, University of Napoli Federico II, Strada Comunale Cinthia, 26, Napoli 80126, Italy
[c] Institute on Polymers Composites and Biomaterials, National Research Council, Via Campi Flegrei, 34, Pozzuoli 80078, Italy
[d] C.R.A. S.r.l., Calle Giovanni Legrenzi, 2, Venice, VE 30171, Italy

ARTICLE INFO

*Keywords:*
PH sensing hydrogel
Colorimetric tool
Milk and chicken freshness
Food spoilage
Shelf-life

ABSTRACT

There is a growing interest in soft-matter sensors at the research and application level. Colorimetric hydrogel-based sensors can work as smart tools for the fast, simple, and low-cost monitoring of food freshness and spoilage. Herein we developed a hydrogel pH indicator working from pH 2–12 with a specific colorimetric pattern. A fast-responsive, easily formed and mouldable hydrogel was obtained by adding a minimal amount of a single pH-sensitive dye to an agar matrix. Optical, mechanical, and morphologic characteristic of the hydrogel were examined in detail. An easy-to-use smartphone app ensures color tone capture and correlation of color changes to pH levels. Practical applications of the versatile gel sensor were tested in solution and in the gaseous phase. The sensor was employed to assess the freshness of milk samples and to monitor the volatile basic nitrogen compounds resulting from packaged chicken spoilage.

## 1. Introduction

Intense scientific and industrial research has been conducted to develop smart sensors monitoring food freshness and spoilage. Hydrogels are three-dimensional networks consisting of polar functional groups swollen with a large amount of water. Due to their water content, porosity and consistency, hydrogels enable a wide range of uses, from tissue engineering (Lee & Mooney, 2001; Van Vlierberghe et al., 2011) to food science (Mezzenga et al., 2005). Their sensing ability and stimuli-responsiveness to light, pH, temperature, and solvents is well established and increasingly exploited (Sun et al., 2021). Colorimetric gel sensors are a class of flexible, mouldable devices able to change their colour and absorbance spectrum under specific stimuli. They can work as miniaturized real-time analytical devices providing a fast, simple, and low-cost response to parameters related to the freshness and spoilage of foods.

Many sensitive and rapid pH indicators integrated in a soft aqueous matrix have been proposed for food applications (Abbas & Dawood, 2023; Diana et al., 2020; Rosita Diana et al., 2021; McCoy et al., 2006; Wang et al., 2016). The pH parameter is an excellent indicator for monitoring the freshness, spoilage and correct storage of foods and drinks, applied to the food itself or to secondary spoilage products.

The spoilage produces a pH decrease in some foods, (Korkeala et al., 1990). On the other hand, many types of air pollutants are produced and released during food degradation processes, known as volatile organic compounds (VOCs): carbonyl compounds, S compounds, N compounds. Protein foods are affected by bacteria and microorganisms decomposing proteins and amino acids into volatile compounds (Baston et al., 2008). Degradation of proteins and other nitrogen-based compounds cause accumulation of organic amines (such as phenyl-ethylamine, tyramine, trimethylamine, ethylamine) commonly known as total volatile basic nitrogen (TVB-N) content (Bekhit et al., 2021).

Optical sensors based on food spoilage indicators have proven to be practical methods for monitoring food freshness, due to their simple and fast operation. (Ding et al., 2022; Liu et al., 2020; Lu et al., 2020; Luo et al., 2021). Smart packaging consists of a small tag attached to the food packaging monitoring the freshness or condition of packaged food (Ghaani, Cozzolino, Castelli, & Farris, 2016). An on-pack indicator able of changing color and/or fluorescence (Jia et al., 2019; Roy et al., 2019; Ye et al., 2022; Zeng et al., 2022; Zhang et al., 2024) reacting with the

* Corresponding author.
*E-mail address:* rosita.diana@unina.it (R. Diana).

https://doi.org/10.1016/j.jfca.2024.106667
Received 6 July 2024; Received in revised form 18 August 2024; Accepted 19 August 2024
Available online 23 August 2024

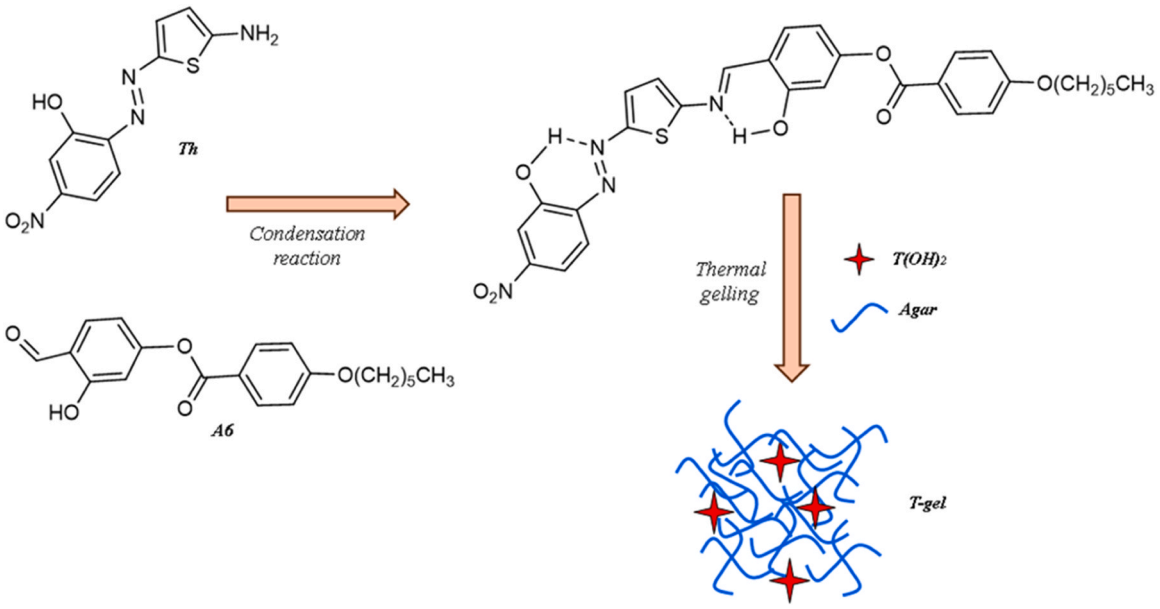


**Fig. 1.** Schematic representation of the synthetic route to the chromophore $T(OH)_2$ and to the hydrogel T-gel.

VOCs generated by packaged foods is the perfect example of smart packaging. A naked-eye response, possibly processed via a mobile device, is desirable. Among VOCs, the TVB-N fraction is a measure of food freshness that can be captured by a pH-sensitive molecule. Sensitive, fast and intensely colored pH indicator molecules, immobilized in a suitable polymer substrate, are a great example of intelligent packaging. High-performance smart sensors can be developed by combining the sensitive response of colorimetric pH indicators with the exceptional porosity and swelling ability of hydrogels.

Here we developed a hydrogel-based pH sensing system, with a specific color display between pH=2 and 12. The use of agar as a non-toxic and low-cost polysaccharide was due on its unique ability to form strong gels in aqueous solutions. A responsive porous hydrogel easily molded into patches or tablets was obtained by co-gelling a single pH-sensitive dye and agar. The novel dye called T(OH)2 (Fig. 1 and Section 2.1) has been fully characterized, obtaining large absorbance coefficients and colorimetric variation over a wide pH range. The physical properties, mechanical strength, and morphology of the hydrogel sensing tool (T-gel in Fig. 1) were investigated. A mobile app based on specific software that captures color changes as a function of pH levels has demonstrated the effectiveness of T-gel as a commercial pH test. The performance of the sensor was tested in different environments, both in solution and in the gaseous phase. As practical applications, we verified the sensor's ability to monitor food freshness through contact with untreated milk samples at different storage times. On the other hand, we investigated the sensor's ability to monitor chicken spoilage resulting from TVB-N in packaging as a function of time.

## 2. Materials and methods

Agar for microbiology was purchased from Neofroxx GmbH (Einhausen, Germany) code 20767.232. Solvents and other commercially available starting products were of reagent grade and used as supplied, without further purification. They have been purchased from Sigma Aldrich (Milan, Italy). Ultrapure water was used throughout the experiment (Millipore USA, 18.2 MΩcm at 25 °C). NMR spectra were recorded in $CDCl_3$ with a Bruker Advance II 500 MHz apparatus (Bruker Corporation, Billerica, MA, USA). For $^{13}C$ NMR spectra the experiment was a DEPTQ (Distorsionless Enhancement by Polarization Transfer Including the Detection of Quaternary Nuclei) polarization transfer with decoupling during acquisition using a shaped pulse for a 180-degree pulse on the f1 channel. For mass spectrometry measurements, the samples were analysed by direct flow injection using an LTQ Orbitrap XL mass spectrometer (Thermo Scientific, San Jose, CA, USA), operating in positive and/or negative ionization mode. The Orbitrap mass analyser was calibrated according to the manufacturer's directions using a mixture of caffeine, methionine-arginine phenylalanine-alanine-acetate (MRFA), sodium dodecyl sulphate, sodium taurocholate, and Ultramark 1621. Data were collected and analysed using the software provided by the manufacturer. A Crison pHmeter GLP 22 was employed for all pH measurements.

### 2.1. Synthesis of $T(OH)_2$ dye

The novel dye $T(OH)_2$ depicted in Fig. 1, 3-hydroxy-4-(((5-(2-hydroxy-4-nitrophenyldiazenyl)thiophen-2-yl)imino)methyl)phenyl-4-(hexyloxy)benzoate, was obtained by reaction of the aminic group of the azo compound Th (2-((5-aminothiophen-2-yl)diazenyl)-5-nitrophenol, 10 mmol) (Borbone et al., 2009) and the carbonyl group of the aldehyde A6 (4-formyl-3-hydroxyphenyl 4-(hexyloxy)benzoate, 10.5 mmol) (Diana et al., 2019) in 15 mL of chlorobenzene. The solution was stirred gently at reflux for 3 hours and the crude product was recovered by removing the solvent under vacuum. The obtained dark solid was was chromatographed on Florisil 60/100, using chloroform as the eluent, and collecting the overhead fractions. The fractions were recovered by removing solvent in vacuo. The red precipitate was washed twice with ethylic ether, then crystallized from chloroform/hexane into a brick red microcrystalline powder. Yield: 35 %. $^1H$ NMR (500 MHz, $CDCl_3$, 25 ∘C, ppm): 0.93 (t, 3 H), 1.36 (m, 2 H), 1.56 (m, 2 H), 1.82 (m, 2 H), 2.04 (m, 2 H), 4.06 (t, 2 H), 6.94 (m, 2 H), 6.99 (t, 2 H), 7.19 (d, 1 H), 7.44 (d, 1 H), 7.74 (d, 1 H), 7.89 (m, 3 H), 8.15 (d, 2 H), 8.70 (s, 1 H), 11.57 (s, 1 H), 12.41 (s, 1 H). Hard copy of $^{13}C$ NMR in Fig. S1. Elemental analysis calculated (%) for $C_{30}H_{28}N_4O_7S$: C, 61.21; H, 4.79; N, 9.52; found: C, 61.26; H, 4.81; N, 9.60. MALDI-TOF MS (*m/z*): 588.17, found [M-H]: 587.03.

### 2.2. Sensing agar hydrogel (T-gel) preparation

The T-gel samples were prepared by mixing 6 % g/mL of agar powder with milli-Q water brought to a boil for 5 min reaching approximately 100 °C while stirring until complete dissolution. After this time, $T(OH)_2$ was added dissolved in acetone (0.02 M), at 2 % w/w

on the dry agar. Acetone was removed heating the mixture for another 2 minutes at 100 °C. The obtained solution was then cooled in air pouring it into cylindrical moulds. Pirex glass micro beaker was employed, obtaining 15 mm (diameter) x 12 mm (height) transparent round samples. The gelation was allowed to proceed at room temperature (Bertasa et al., 2018).

### 2.3. Hydrogel characterization

#### 2.3.1. Fourier transform infrared spectra (FTIR)

FTIR spectra were collected in the attenuated total reflection (ATR) mode using a single reflection ATR accessory (UATR from Perkin-Elmer, Newark, NJ, USA). This unit was equipped with a diamond crystal as internal reflection element (IRE) and two ZnSe crystals as transfer elements. The IRE had horizontal geometry, and an angle of incidence of 45°. The optimum wavenumber range for the present configuration was 4000–650 $cm^{-1}$. The ATR accessory was equipped with a pressure transducer on the crystal tip to ensure reproducible and uniform sample-to-IRE contact. Measurements were taken by a Spectrum 100 interferometer (Perkin-Elmer), equipped with a wide-band deuterated triglycine sulfate (DTGS) detector and a Ge on KBr beam splitter. The frequency scale was internally calibrated to 0.01 $cm^{-1}$ using a He–Ne reference laser. 16 scans at a resolution of 2 $cm^{-1}$ were averaged to improve the signal-to-noise ratio.

#### 2.3.2. Scanning electron microscopy (SEM)

SEM analyses were performed using a scanning electron microscope, Thermo Phenom XL by Zeiss (Carl Zeiss NTS GmbH, Oberkochen, Germany), on the dried spun films. The operating voltage was from 15 kV to 10 kV.

#### 2.3.3. Swelling ratio and water retention ratio

T-gel samples were immersed into distilled water to obtain equilibrium swelling. Dried samples were obtained under a hot air oven at 50 °C for 2 hours (Jyoti Chaudhary et al., 2020; Lv et al., 2019).

To calculate the water retention ratio (WRR) gel samples were immersed into deionized water to acquire different swelling ratio (SR) at room temperature and at pH=7. The samples were taken out of the water at time intervals, and the excess surface water was gently removed with paper. SR was calculated by the following equation: SR(%)=(Wt-Wd)/Wd x 100, where Wt and Wd represent the weight of the swollen sample at t time and the initial weight of the dry sample, respectively. Reached the equilibrium swelling at room temperature and at pH=7 the gel samples were used in the following water retention experiments. The WRR experiments were performed at room temperature and at pH=7 by keeping the swollen samples in the open air (relative humidity about 40 %) for different times. WRR was evaluated according to the following equation: WRR(%)=(Wt-Wd)/Wd x 100, where Wt and Wd represent the weight of the swollen sample at t time and the weight of the dried sample, respectively.

#### 2.3.4. DSC Measurements

DSC experiments were performed with a Hitachi DSC 200 under nitrogen purge gas. T-gel samples were subjected to heating and cooling cycles consisting of 1 min hold at 20 °C, heating to 100 °C at 5 °C/min, hold at 100 °C for 1 min and cooling to 10 °C at 5 °C/min. The melting and gelation temperature and enthalpy were determined from the thermograms.

#### 2.3.5. Mechanical properties

T-gel samples were obtained cylindrical in shape with dimensions of 30 mm (diameter)×12 mm (height). Compression tests (stress/strain) were done on an Instron 5566 at a crosshead speed of 1 mm/min up to an extension of 2 mm (breaking of gel) using a 100 N load cell.

### 2.4. Preparation of solutions of $T(OH)_2$ dye for absorbance experiments

UV–visible absorption spectra were recorded by a JASCO F-530 spectrometer (scan rate 200 nm/min, JASCO Inc., Easton, MD, USA) on $10^{-5}$ M in commercial buffer solutions. The dye solutions used to measure absorbance as a function of pH were prepared by dissolving T $(OH)_2$ at the appropriate volume ratio of water: acetone (3:1 solutions or 1:6 solutions) and using Britton-Robinson buffer solutions. In both cases, the concentration was fixed at $1.5{\cdot}10^{-5}$ M. After mixing for a few seconds, the absorption spectra were recorded at room temperature. The solutions of both series were kept at 25 °C in daylight for ten months. After that time, colour perceived and absorption spectra show an unaltered pattern.

### 2.5. pH sensing test of T-gel in aqueous phase

The colorimetric performance of the hydrogel indicator was evaluated by immersion of T-gel tablets in different water solution buffered from pH=2 to 12. Each hydrogel sample were kept for 10 min in immersion, gently dabbed with paper, and photographed to evaluate pH value vs. colour by a smartphone app. Different response times were evaluated. In buffered water the color shows clearly starting from 3 min of immersion.

### 2.6. pH sensing test of T-gel in gaseous phase

The colorimetric sensing ability of T-gel was evaluated in presence of $NH_3$ vapour. T-gel tablets were kept in contact with $NH_3$ vapour of a saturated solution in a sealed vial. Different exposure times were evaluated on each sample, and the colorimetric response recorded at 5", 10", 15", 20", 25" and 30". The samples were photographed immediately after exposure and after 2 hours, observing unaltered color. Experiments were conducted to test the reversibility of the colorimetric response to gaseous analytes using saturated solutions of $NH_3$ and HCl. The samples were exposed alternately for 30" to $NH_3$ and HCl in a sealed vial for five equivalent cycles, recording the restoration of CIE colorimetric coordinates in each cycle.

### 2.7. T-gel colour parameters

The colour changes of T-gel at various pH values were investigated by employ of the CIE 1931 RGB (Red, Green, Blue) colour space. CIE calculation was performed by the mobile app named "RGB Colour Detector". The RGB colour intensity was recorded by holding the smartphone camera (Samsung S23) approximately 1 cm from each sample in daily light. Each sample was evaluated in triplicate by parallel test. The statistical analysis was performed by the ANOVA by SPSS 22.0 (SPSS Statistical Software, Inc., Chicago, IL, USA) package included in Origin 8.5.0 SR1 with the confidence interval set to 95 % to determine the significant difference between specific means.

### 2.8. Application of T-gel as colorimetric sensor for chicken spoilage

T-gel tablets were placed in commercial PS trays each containing two fresh chicken thighs (chicken weighs are approximately 300 g, the dimensions of the PS tray are approximately 20×10 cm in all the experiments). The packages were wrapped in a PVC/PVDC copolymer (Saran) cling film for food use. Experiments were carried out to monitor the food spoilage at recommended storage conditions (4 °C) and at accelerated stability conditions (room temperature). All samples were evaluated in triplicate by parallel test. Three samples were kept for 10 days at 4 °C and three samples were kept for 4 days at 25 °C. Photographs of the packages were taken at specific time intervals. Color analysis was performed using the smartphone app and correlated with storage time. To verify the accuracy of the developed method, the pH of the meat of each sample stored at 25 °C was measured.Ten grams of grinded chicken

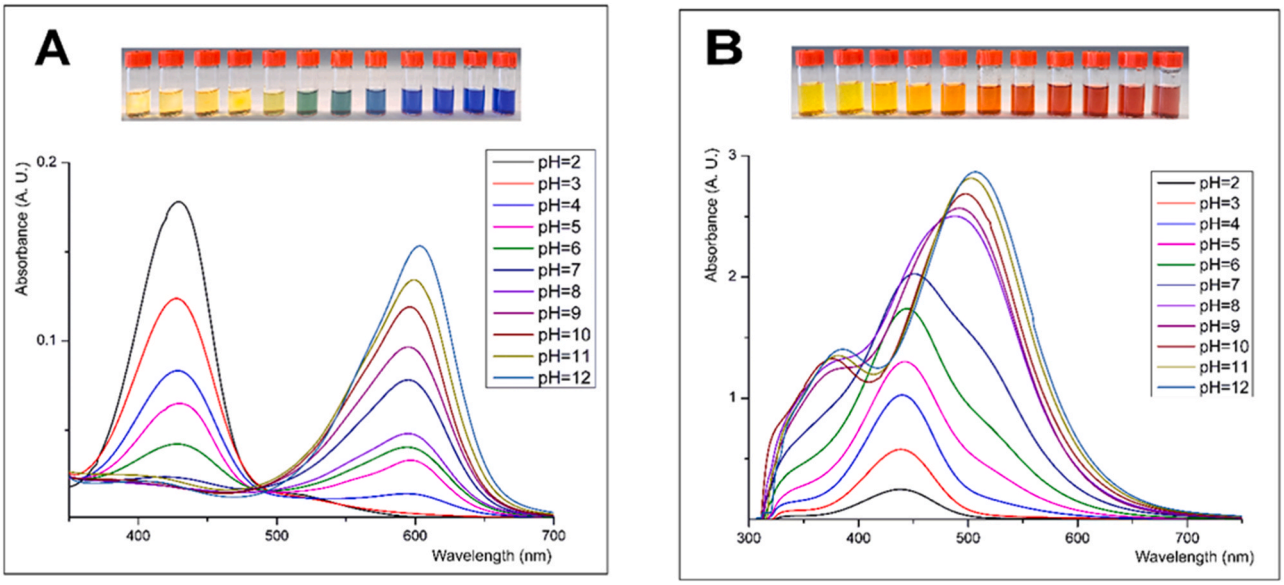


**Fig. 2.** Experimental UV–vis absorption spectra of $T(OH)_2$ recorded in (A) mainly-water (water/acetone 3:1) and (B) mainly-organic (water/acetone 1:6) buffered solutions as a function of pH.

sample was homogenized in distilled water and the pH of the mixture was measured by the electronic pH meter.

### 2.9. Application of T-gel as colorimetric sensor for milk freshness

T-gel tablets were placed in vials with a commercial sample of low-fat fresh pasteurized milk (3 mL). Milk samples were stored at 4 °C for 1 h ours (listed as "fresh"), at 25 °C for 24 hours ("spoling"), and at 25 °C for 48 hours ("spoiled"). The samples described as fresh (good quality), spoiling (approaching spoiled), and spoiled (poor quality) correspond to samples at pH=6.7, pH= 5.5, pH=4.4 respectively (measured by the electronic pH meter). The method was also tested on milk model samples prepared by adding a Britton-Robinson buffer to obtain quite the same acidity levels of the real samples. A fourth model sample was added to them of a pathogenic ("mastitic") milk at pH=7.5, obtained by buffering the same fresh milk sample. The pH values were verified in each sample by the electronic pH meter. The tablets were kept immersed in milk for 10 min at 25 °C, then gently washed, dabbed with paper, and photographed. All samples were evaluated in triplicate by parallel test. Color analysis was performed using the smartphone app and correlated with storage time.

### 2.10. Theoretical calculations

Calculations were performed by the Density Functional Theory (DFT) approach within the Linear Combination of Atomic Orbitals (LCAO) framework, where each molecular orbital is expanded into a set of Gaussian Atomic Orbital (GAO) functions centered at the nuclei positions. The HOMO analysis was derived from ground state calculations, the LUMO evaluation was performed considering the first excited state using the Time-Dependent Density Functional Theory (TDDFT) formalism. The software used was ORCA version 5.0.3 (Neese, 2012). A global hybrid B3LYP functional (Becke, 1992), which includes a fraction of exact Hartree-Fock exchange, was employed as in our previous work (Gentile et al., 2018; Gentile et al., 2018). Grimme's D3 empirical correction was adopted for consistent evaluation of dispersion interactions (Grimme et al., 2021). We used Double-ζ Basis sets (optimization) and Triple-ζ Basis sets (TD-DFT) specifically the def-SVP and def2-TZVPP from the Karlsruhe group (Weigend, 2006). These basis sets have been tested in several of our previous works (R. Diana et al., 2021; Diana et al., 2020) and are among the best choices in terms of computational performance. The thermodynamic part to derive the dissociation energy of the two hydroxyl protons was obtained from frequency calculations, using the analytical Hessian available in ORCA.

## 3. Results and discussion

### 3.1. Design and pH colorimetric response of T(OH)$_2$

Many pH-sensitive colorimetric dyes have applications as indicators integrated into soft sensors. Our novel dye named $T(OH)_2$, 3-hydroxy-4-(((5-(2-hydroxy-4-nitrophenyldiazenyl)thiophen-2-yl)imino)methyl) phenyl-4-(hexyloxy)benzoate, was synthetised as summarised in Fig. 1. The two H-bonding hydroxyl substituents prevent isomerization of the azo bridge and stabilize the imine bond, even in strong acidic and alkaline environments. In addition, the OH groups improve solubility in water-containing solvents and in the agar gel. On the other hand, the $(CH_2)_5CH_3$ alkyl chain increases the flexibility and solubility of the chromophore in organic solvents.

The broad modulation of the colorimetric pH response of $T(OH)_2$ is related to the highly conjugated chromophore moiety constituted by the phenol-(N═N)-thiophene-(C═N)-phenol scaffold. The high molar absorbance coefficient is mainly due to the Th precursor, 2-((5-aminothiophen-2-yl)diazenyl)-5-nitrophenol, examined in a previous work (Diana et al., 2024). $T(OH)_2$ molecule works as a pH indicator detecting the presence of protonating or deprotonating agents by reacting with $H^+$ or $OH^-$. Protonation/deprotonation equilibria involve the two OH functions. When the protonation occurs to both sites, the indicator shows the yellow color, when the deprotonation occurs to both sites, the conjugate base shows the different color (blue in mainly-acetone solution, magenta in mainly-water solution). Deprotonation can be even partial. As discussed in Sect. 3.2, the proton lost from the hydroxyl group near the C═N bond produces a first chromatic change that overlaps with that due to the deprotonation of the hydroxyl group near the N═N bond. The two effects contribute to a broader colorimetric display from pH=2–12.

$T(OH)_2$ dye reversibly works between pH=2 and pH=12 both in ambient and refrigerated conditions. The intensely colorful solutions of $T(OH)_2$ give a strong absorption band (magnitude of molar absorbance from $10^3$ to $10^4$) in the visible spectrum both in mainly-water (water/acetone 3:1) and mainly-organic (water/acetone 1:6) solutions. In mainly-acetone solutions the color clearly changes from a yellow tone to

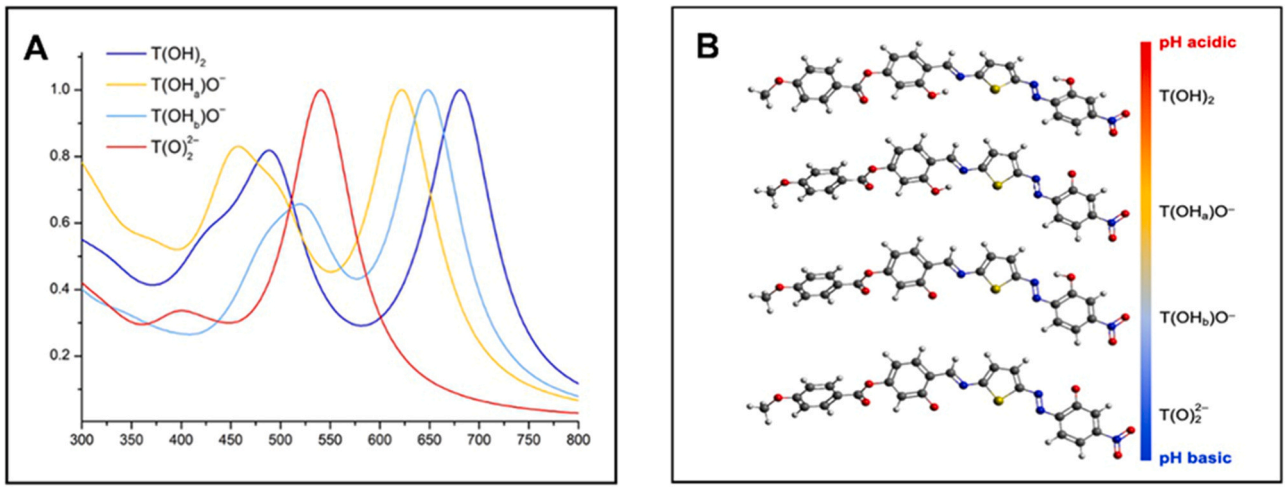


**Fig. 3.** (A): UV–vis absorption spectra calculated by TD-DFT analysis in different protonation states. A Lorentzian fitting is adopted with FWHM of 80 nm. (B): the related four structures at different levels of deprotonation in different pH conditions. The structures are in energetic order from top to bottom.

a blue tone depending on the pH (Fig. 2 A). In mainly-water solutions the color gradually turns from yellow to orange and finally to purple depending on the pH (Fig. 2 B). In this case, the main absorption peak undergoes a red-shift and the whole absorbance curve changes its shape at alkaline pH values. The experimental maximum absorption wavelengths and the absorption molar coefficients as a function of pH are reported for both systems in Table S1.

### 3.2. Theoretical approach to the $T(OH)_2$ system

The structure of $T(OH)_2$ was preliminarily analyzed by varying the configuration of the C-C-C═N and N═N-C-C dihedrals (Fig. S2) to obtain the lowest energy torsional configuration. The best configuration maximizes the hydrogen bonds interaction between O–H–N sites. The structure was subsequently optimized in terms of geometrical relaxation, obtaining a fully protonated molecules corresponding to the acidic conditions. Other three structures were considered, by deprotonation of the OH near the iminic group ($T(OH_a)O^-$), deprotonation of the OH near the azo group ($T(OH_b)O^-$), deprotonation of both sites ($T(O)_2^{2-}$), see Fig. 3 B. The complete optimization of all structures was performed through the evaluation of the analytical gradients. The frequency calculations were employed to determine the vibrational modes of the molecule. From the analytical Hessian matrix (the matrix of second derivatives of the energy with respect to nuclear coordinates) the vibrational frequencies were obtained and used to compute the thermodynamic functions of the differently deprotonated structures. ΔG of the first deprotonation reaction illustrates the different reactivity of the proton with the solvent, emphasizing the fact that the two protons are not equivalent. Specifically, the deprotonation reaction involving the proton b is slightly favorite in energy respect to the proton a (0.12 kcal/mol difference).

Interestingly, the energetic factors are reflected in the absorption pattern derived by TDDFT calculation (see Fig. 3 A). Each spectrum exhibits distinct peaks, analyzed in detail in the Supp. Mat (Sect. S1). A progressive red-shift of the HOMO-LUMO transition from the acidic form to the alkaline fully deprotonated form is recorded. The two monodissociated states, $T(OH_a)O^-$ and $T(OH_b)O^-$ can be distinguish each other in the calculated absorbance spectrum. The form with proton Ha is slightly more stable and is characterized by a blue-shifted transition. The different activation of the two protons as the pH varies leads to the desirable broader colorimetric pattern.

### 3.3. Formation of T-gel by thermal treatment

Given its importance in the biomedical field and in the food industry, in-depth studies have been carried out to clarify the gelation mechanism of agarose (Tokita M Fau - Hikichi & Hikichi; Zhou et al., 2004). Agarose forms thermoreversible gels in water and gelation can take place only when parts of the chains form ordered regions (junctions). A characteristic of agarose gels is massive thermal hysteresis, attributed to the formation of large stable aggregates at temperatures much higher than those at which individual helices form on cooling. The mechanism provides that in solution at high temperatures the agarose chains are in a random coil conformation (Graham et al., 2019; Tako & Nakamura, 1988) responsible for the low viscosity plateau. The increase in viscosity at about 50 °C is due to the formation of double helices of agarose chains assisted by formation of intramolecular hydrogen bonds. The H-bonds stabilize the double helices and increase the stiffness of the chains. Finally, the sharp increase of viscosity at around 40 °C (TV transition) can be attributed to the aggregation of the double helices of agarose into a gel. While at low concentrations (below 2 % w/w) double-helix formation is preceded by spinodal de-mixing into polymer-rich and solvent-rich regions, at high concentrations gelation occurs directly from a homogeneous solution (Fernández et al., 2008).

In our study, the translucent cylindrical hydrogel samples were obtained from 6 % w/w (agar/water) solution without employ of external gelation additives. Six hours gelling time resulted appropriate to achieve well-formed free-standing hydrogels. The addition of the dye solution ($T(OH)_2$ 2 % w/w on the dry agar) to what is supposed to be a solution should provide a micro homogeneous gelled product. The formation of H-bonds between –OH and –COOH groups of the agar matrix and the dye presumably leads to an interpenetrating network, after the appropriate gelling time (Baroutaji et al., 2019). The absence of dye-rich microdomains may positively affect the sensing performance of the hydrogel both in the response time and in the color perception. In addition, increasing the agar concentration contributes to an increase in the crosslink density which provides a gel with great strength (Augst et al., 2006).The Winter & Chambon theory (Chambon & Winter, 1987) provides data on the gelation time and temperature of such systems. The thermal behaviour of T-gel samples was investigated by differential scanning calorimetry. Fig. S3 shows the thermograms obtained on heating and subsequent cooling a T-gel sample. In Fig. S3 A the broad signal peaked at 88.0 °C corresponds to the melting of the hydrogel, (ΔH=4.35 J/g). In Fig. S3 B, the gel formation peak is observed at 30.1 °C (ΔH=1.93 J/g). These results agree with literature data for agar gel specimen at high agar concentration (Fernández et al., 2008), where

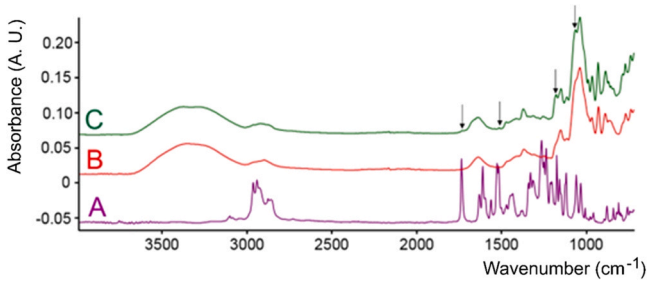


**Fig. 4.** FTIR spectra spectra in the 4000 – 700 $cm^{-1}$ range of (A) $T(OH)_2$, (B) agar, (C) T-gel.

gelation occurs directly from the homogeneous solution.

### 3.4. FTIR analysis

The spectrum of the pure dye $T(OH)_2$ is shown in Fig. 4 A. In the high-frequency side it displays a weak feature at 3100 $cm^{-1}$ due to H-bonded NH groups and a multicomponent pattern in the 3000 – 2800 $cm^{-1}$ range due to the $CH_2/CH_3$ stretching modes. Below 1800 $cm^{-1}$ a rich pattern of sharp, well resolved peaks is observed, characteristic of the different functional groups of the molecule. In particular, the $\nu$(C═O) of the substituted phenyl benzoate is found at 1736 $cm^{-1}$, and the associated C–O–C vibration at 1264 $cm^{-1}$. The partially resolved components at 1250 and 1236 $cm^{-1}$ are likely contributed by the $\nu$(C–O) vibration of the terminal alkyl-aryl ether. A doublet at 1524/1515 $cm^{-1}$ and a component at 1328 $cm^{-1}$ are assigned, respectively, to the antisymmetric and symmetric stretching modes of the terminal $NO_2$ group. Various peaks in the 1660 – 1400 $cm^{-1}$ range and between 900 and 600 $cm^{-1}$ are mostly due to in-plane and out-of-plane deformation modes of the substituted aromatic rings (Bellamy, 1975; Roeges, 1995). Overall, the IR spectrum confirms the postulated molecular structure of the dye. The sharpness and the apparent splitting of several peaks (crystal-field splitting) suggests the occurrence of long-range ordering.

The spectrum of pristine agar is reported in Fig. 4 B. It displays a broad band in the 3700–3000 $cm^{-1}$ range mostly due to the $\nu$(HOH) modes of residual water plus unresolved $\nu$(OH) and $\nu$(NH) contributions. The complex profile centered at 2920 $cm^{-1}$ is due to the CH stretching modes; a well-resolved band at 1650 $cm^{-1}$ is related to the $H_2O$ bending with possible contribution from residual peptide linkages (amide I mode). Prominent features at 1374, 1070 and 1039 $cm^{-1}$ are respectively due to $CH_2$ scissoring/$\nu$(S═O) in sulfate ester, $CH_2$ bending of the pyranose ring and C–O–H bending (Rochas et al., 1986; Shahnaz et al., 2019). Finally, the spectrum of agar with the dye (T-gel at 2 % w/w, Fig. 4 C) displays the same features of the neat agar sample plus some new peaks originating from the additive (marked by arrows in Fig. 4 A) and very weak owing to the low amount of dye in the mixture. The marked peaks in Fig. 4 A are recorded at 1730, 1515, 1178, and 1065 $cm^{-1}$. These peaks are detected at frequencies close to those of the pristine dye, while the carbonyl displays a redshift of 6 $cm^{-1}$. This effect can be attributed to molecular interaction of the H-bonding type with water and/or agar. All the bands of the dye in the hydrogel display a well-defined, mono-profile structure, as opposed to the complex multi-component pattern observed in the pristine dye. This suggests the suppression of crystal-field effects, i.e. the absence of crystalline order in the dye. The spectroscopic analysis demonstrates that in the agar/dye mixture the hydrogel structure remains unaltered, and the dye is successfully and permanently incorporated into the gel. In fact, the significant peak shift of the carbonyl and the absence of long-range order suggest the occurrence of H-bonding interactions with water and/or agar (H-bonding association of –OH groups), which promote dispersion and suppress crystallization.

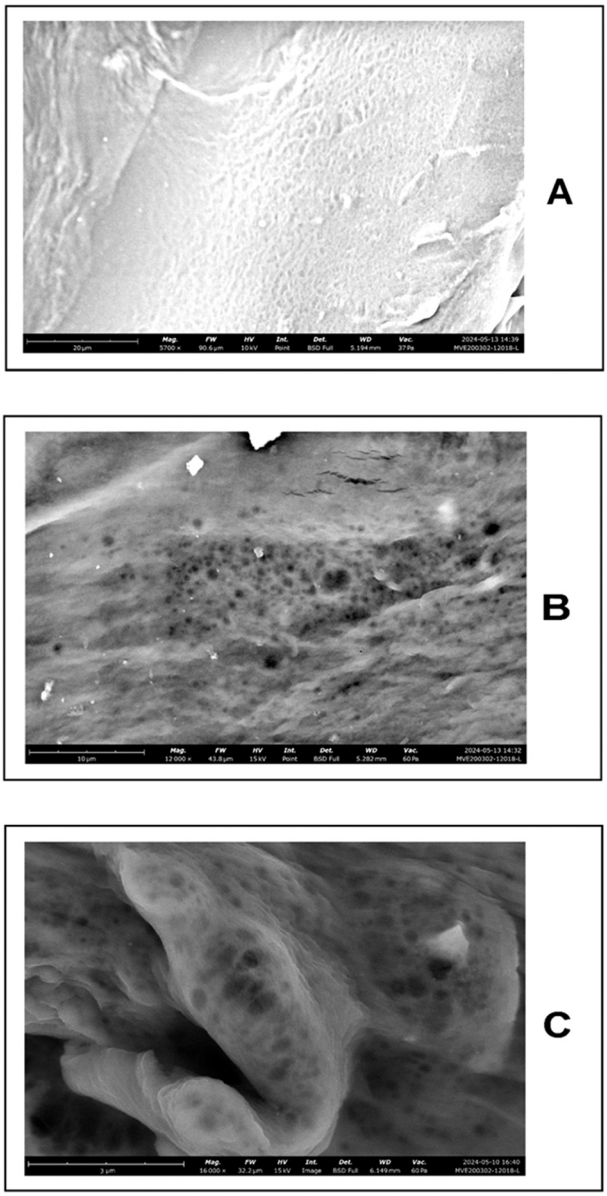


**Fig. 5.** SEM micrographs of the hydrogel surfaces at different magnifications and scale bars: 5700x (A); 12000x (B); 16000x (C).

### 3.5. Compressive strength of T-gel

Maximum stress is an index reflecting the extent of resistance offered per unit of contact area towards compression to the gel deformation (before breaking). In the case of T-gel samples, a set of measurements were recorded, and the medium values gave results consistent with other thermally gelled agar hydrogels effectively employed for sensing (Banerjee & Bhattacharya, 2011). Computing the average value, we had not observed breaking of gels up to an applied strain of 120 KPa, corresponding to a compression of 20 %, see graph stress vrs. strain in Fig. S4 A.

### 3.6. Swelling behaviour of hydrogels

Swelling ratio (SR) and water retention ratio (WRR) are key parameters for the hydrogels (Lv et al., 2019) as they measure the ability to maintain the water reserve necessary to act as a sensor. Both SR and WWR are function of time and depend on two processes: penetration of solvent molecules into the inner free space of hydrogels; relaxation and

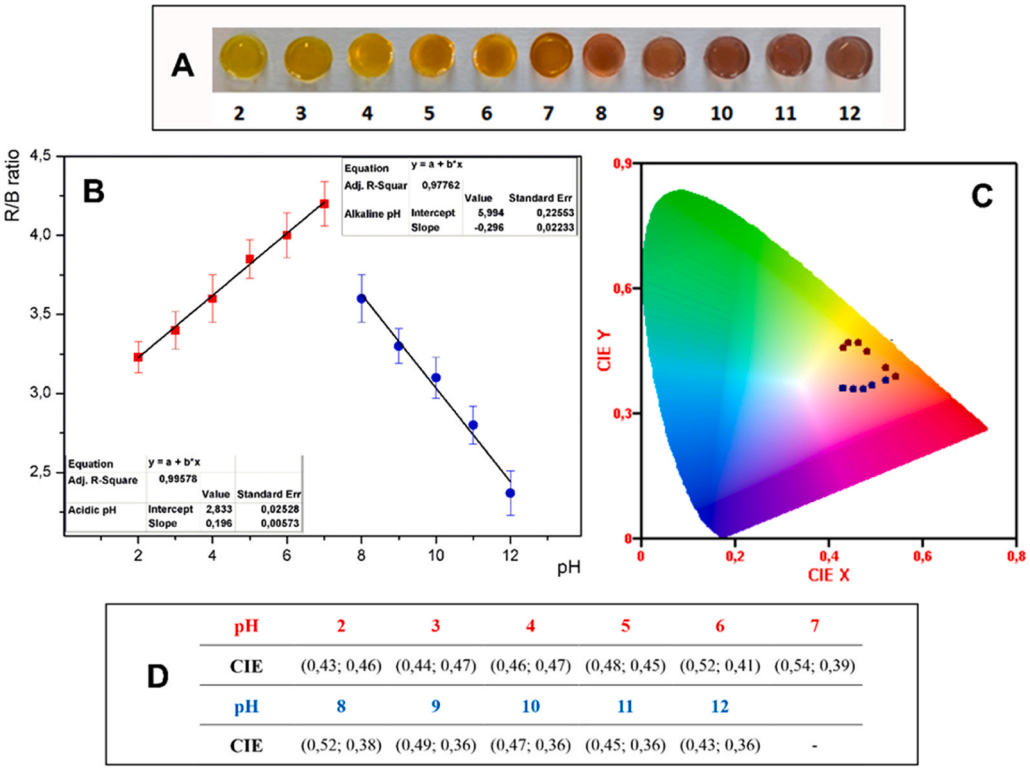


D

| pH | 2 | 3 | 4 | 5 | 6 | 7 |
|---|---|---|---|---|---|---|
| CIE | (0,43; 0,46) | (0,44; 0,47) | (0,46; 0,47) | (0,48; 0,45) | (0,52; 0,41) | (0,54; 0,39) |
| pH | 8 | 9 | 10 | 11 | 12 | |
| CIE | (0,52; 0,38) | (0,49; 0,36) | (0,47; 0,36) | (0,45; 0,36) | (0,43; 0,36) | - |

**Fig. 6.** (A): Photograph in natural diffused and shadowed light displaying the gradual colour changes of T-gel samples immersed in water buffered solutions from pH=2–12. (B): R/B plot of T-gel colour as a function of pH. The calibration curve was obtained by a smartphone based colorimetric method. (C): CIE diagram: red points related to the values in the pH range 2–7; blue points related to the values in the pH range 8–12. The related CIE coordinate values are reported in the table in panel (D).

expansion of the polymer chains after absorbing the solvent. For T-gel immersed in water for 10 min, SR reach 105 g/g; 1 hour later SR rises to 1026 g/g; after 6 hours the equilibrium swelling is reached with the SR around 3900 g/g (see graph SR% vrs. time in Fig. S4 B). The T-gel sample after reaching the equilibrium swelling at pH=7 and 25 °C was reused in WRR test. Specifically, the WRR parameter of the sample with initial SR 3900 g/g (in air at 25 °C with the humidity of around 40 %) was found to remain around 80 % after 1 day, and still 65 % after 3 days in the same conditions. According with such results, we claim excellent water retention capability of our hydrogel samples (J. Chaudhary, S. Thakur, M. Sharma, V. K. Gupta, & V. K. Thakur, 2020). This implies the possibility of using stable T-gel samples even for long-term pH monitoring.

### 3.7. Hydrogel morphology

The morphology of T-gel was investigated by SEM analysis. In Fig. 5 are shown the SEM micrographs of the hydrogel surfaces acquired at different magnifications: 5700x (Fig. 5 A), 12000x (Fig. 5 B), and 16000x (Fig. 5 C), respectively. The surface of the hydrogels is quite rough, with uneven micropore distribution, rather rounded and of variable dimensions. The porous structure offers an advantage for the use of T-gel as a permeable, “micro-spongy” medium where protonation-deprotonation equilibria easily and rapidly occur.

### 3.8. Colorimetric response of T-gel in buffered aqueous solution

A series of T-gel round tablets were obtained balancing the speed and homogeneity of the response with the long life of the sensor. Due to the excellent performance of T(OH)2, a low dye content (2 % w/w of the dye relative to dry agar) was sufficient for a clear response in all experiments.

The colour display of T-gel at various pH values were investigated by employ of the CIE 1931 RGB colour space (International Commission on Illumination, 1931). CIE colour space is a quantitative link between distributions of wavelengths in the visible spectrum, and physiologically perceived colours in human colour vision. For CIE coordinates determination, T-gel samples were immersed for 1 min in water with a Britton-Robinson buffer at pH from 2–12. The different color shape can be clearly naked-eye detected for intervals of one pH unit (Fig. 6 A). The related CIE coordinates are reported in the table (Fig. 6 D). The colorimetric pattern was monitored by the mobile app named “RGB Colour Detector” on the smartphone camera (Samsung S9). Interestingly, samples from pH=2 to pH=7 display the gradual enhancing in the yellow colour (points marked in red falling in the G/R region of the CIE diagram in Fig. 6 C), while from pH=8 to pH=12 a blue component adds, obtaining the gradual enhancing of the magenta colour (points marked in blue falling in the R/B region of the CIE diagram in Fig. 6 C). This behaviour is associated with the hydrogen transference in the two phenolic functional groups, as discussed in Sect.3.2). The calibration curve in Fig. 6 B was obtained by plotting the varied intensity ratio of R/B with respect to the pH parameter (R. Diana et al., 2021). The plot shows two linear trends, at acidic pH and at basic pH, with a good fitting linear coefficient.

### 3.9. Colorimetric response of T-gel to acid and alkaline vapours

The colorimetric detection capability in the presence of acid and alkaline vapors was tested on a series of T-gel samples. Several hydrogel tablets were kept in contact with $NH_3$ vapor of a saturated solution in a sealed vial. Different exposure times were evaluated, and the colorimetric response recorded at 5”, 10”, 15”, 20”, 25” and 30”. The samples were photographed immediately after exposure (Fig. 7 A) thought after 24 hours they show unaltered color. The sensor, originally yellow

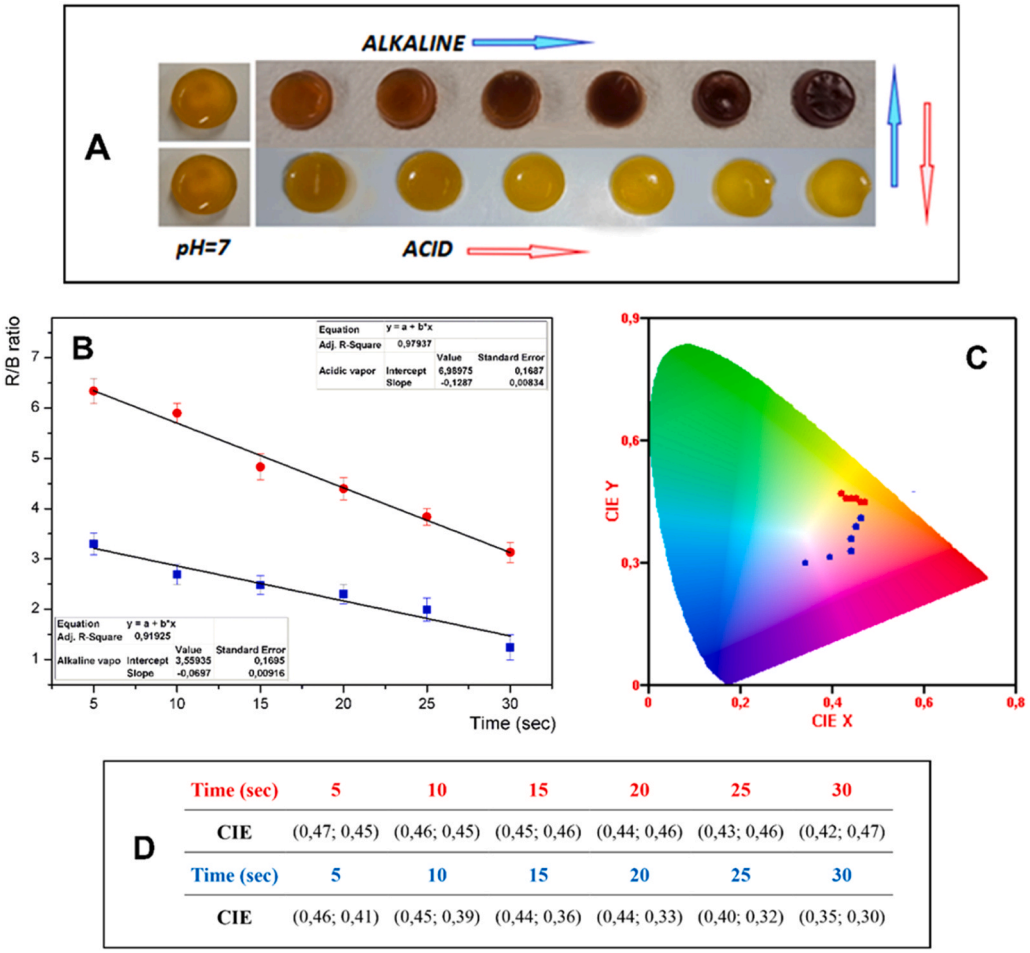


D

| Time (sec) | 5 | 10 | 15 | 20 | 25 | 30 |
|---|---|---|---|---|---|---|
| CIE | (0,47; 0,45) | (0,46; 0,45) | (0,45; 0,46) | (0,44; 0,46) | (0,43; 0,46) | (0,42; 0,47) |
| Time (sec) | 5 | 10 | 15 | 20 | 25 | 30 |
| CIE | (0,46; 0,41) | (0,45; 0,39) | (0,44; 0,36) | (0,44; 0,33) | (0,40; 0,32) | (0,35; 0,30) |

**Fig. 7.** (A): Photograph in natural diffused and shadowed light displaying the gradual colour changes of T-gel samples in contact with $NH_3$ vapour of a saturated solution in a sealed vial (above), and of HCl vapour of a saturated solution in a sealed vial (below) for 5", 10", 15", 20", 25" and 30". (B): R/B plot of colour as a function of the exposure time. The calibration curve was obtained by a smartphone based colorimetric method. (C): CIE diagram: red points related to the values in the pH range 2–7; blue points related to the values in the pH range 8–12. The related CIE values are reported in the table in panel (D).

orange in color (pH=7) records the presence of ammonia even for a minimum exposure time, with a gradual intensification of the purple color. On the other hand, another series of T-gel tablets were kept in contact with HCl vapour of a saturated solution in a sealed vial. Different exposure times were evaluated, and the colorimetric response recorded at 5", 10", 15", 20", 25" and 30". The samples were photographed immediately after exposure (Fig. 7 A) thought after 24 hours they show unaltered color. The sensor, originally yellow orange in color (pH=7) records the presence of HCl even for a minimum exposure time, with a gradual intensification of the yellow color.

The exposure to acid/alkaline vapors causes a strong color modification, more evident in the case of alkaline vapors. The samples exposed to acid vapor display the gradual enhancing in the yellow colour (the points marked in red fall in the G/R region of the CIE diagram of Fig. 7 C); the samples exposed to alkaline vapor display the gradual enhancing in the magenta/violet colour (the points marked in blue fall in the R/B region of the CIE diagram of Fig. 7 C). The calibration curve for the response in gaseous phase showed in Fig. 7 B was obtained by plotting the varied intensity ratio of R/B with respect to the exposure time. Also in this case, the plot shows two linear trends, at acidic pH and at alkaline pH, both with a good fitting linear coefficient. The intensity of the colorimetric response increases compared to what occurs in buffered aqueous solutions, plausibly due to the greater vapor permeability of the porous structure of T-gel (see Sect. 3.7). The colorimetric response is immediate and even reversible. Samples subjected alternately (up to 5 times) to acid and basic vapors return similar color and CIE coordinates (Fig. 7 C). The related CIE values are reported in Fig. 7 D.

### 3.10. Application of the T-gel indicator for monitoring milk freshness

The T-gel system has proven to be a multipurpose tool for controlling the freshness of various perishable foods as it can work in both gas phase and aqueous solution. Milk is a highly perishable liquid food that is vulnerable to bacteria within a few hours out from refrigerator. Temperature variation during storage and handling has crucial influence on microbial activity and product quality (Hu et al., 2022). Milk quality and freshness can be monitor by smell, taste, protein concentration, bacterial count, and pH. As the predominant bacterial substrate in milk is lactose, which is metabolized into lactic acid, the increase in lactic acid concentration corresponds to a decrease of pH due to the bacterial growth. Specifically, pH of milk ranges from 6.8 to 6.5 (fresh) and decreases up to 4.0 as it spoils. Therefore, pH is an excellent indicator of milk freshness (Weston et al., 2020). A simple, fast, and effective pH indicator for milk samples can represent a valuable tool.

T-gel samples were used to monitor milk real samples and milk model samples. Commercial samples of low-fat fresh pasteurized milk were examined at the time of purchase, stored in air at 25 °C for 48 hours, and stored in air at 25 °C for 96 hours. The samples can be described as fresh (good quality), spoiling (approaching spoiled), and spoiled (poor quality) as their pH value corresponds to 6.7, 5.5, and 4.4 respectively. On the other hand, milk model samples were prepared by

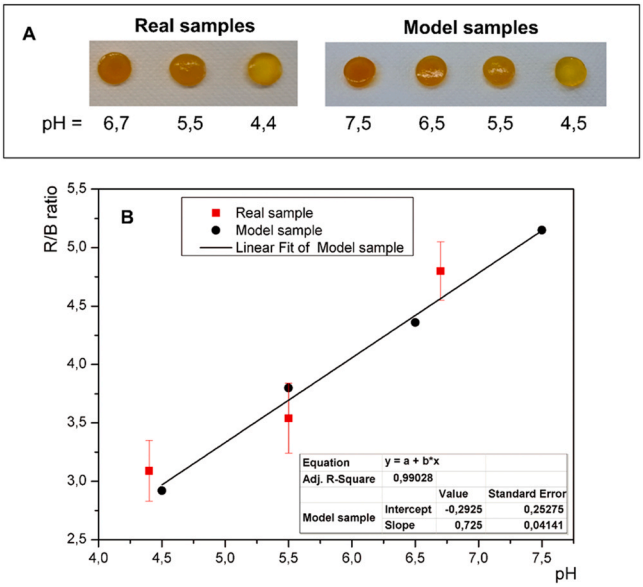


**Fig. 8.** (A): Visual monitoring of model and real milk samples at different pH (photograph in natural diffused and shadowed light) by colour evolution of T-gel immersed 10 min in the samples at 25 °C. (B): Corresponding R/B colour parameters as a function of pH.

adding the suitable buffer solution to the fresh milk samples. The acidity levels of the model samples were set at pH=4.5, pH=5.5, pH=6.5 respectively. An additional milk model sample resembling a pathogenic milk at pH=7.5 was also obtained by adding the suitable buffer solution to the fresh milk sample. The model samples were used to obtain a calibration curve valid in our "milk" system, analogous to the acidic curve of Fig. 6 B. The acidity was measured in each sample by the electronic pH meter.

After immersion in the milk samples for 10 min at 25 °C, the T-gel samples were gently washed, dabbed with paper, and photographed. Upon direct observation (Fig. 8 A), T-gel shows orange colour when immersed in the pathogenic model milk (corresponding to pH=7.5), different shades of orange yellow in the fresh (pH=6.5) and spoiling (pH=5.5) milk, and a neat yellow colour in the spoiled milk (pH=4.5). Unlike in water solutions, in the milk samples the color displays slower due to the specific colloidal nature of milk, and the indicator response is specific. By monitoring the colorimetric response R/B vs. pH in the model samples (including the slightly alkaline sample) we obtained a linear trend with a good fitting linear coefficient (Fig. 8 B, black points). The indicator demonstrated its applicability even for the real milk samples. The colorimetric response of T-gel immersed in the real samples follow the same trend of the calibration curve, confirming replicability and congruence in the examined pH range (Fig. 8 B red points).

### 3.11. *Application of the T-gel indicator for monitoring chicken spoilage*

Due to its relatively low-fat content and nutritional value, flavour chicken meat is widely consumed all over the world (Ghollasi-Mood et al., 2017; Jeon et al., 2010). The product is often marketed in packs. Packaged chicken requires the proper handling and storage to reduce loss of freshness (Grau et al., 2011). Its high perishability and short shelf-life makes it hard to manage (Manouchehri et al., 2020). Therefore, shelf-life estimation of packaged chicken meat is a hot topic. Many relevant articles deal with colour and descriptive sensory analyses of stored chicken meat (Lin et al., 2024). At the consumer level, the chroma of chicken skin is a poor indicator of spoilage, while the smell of raw chicken meat could be a more reliable signal, but effective only in an

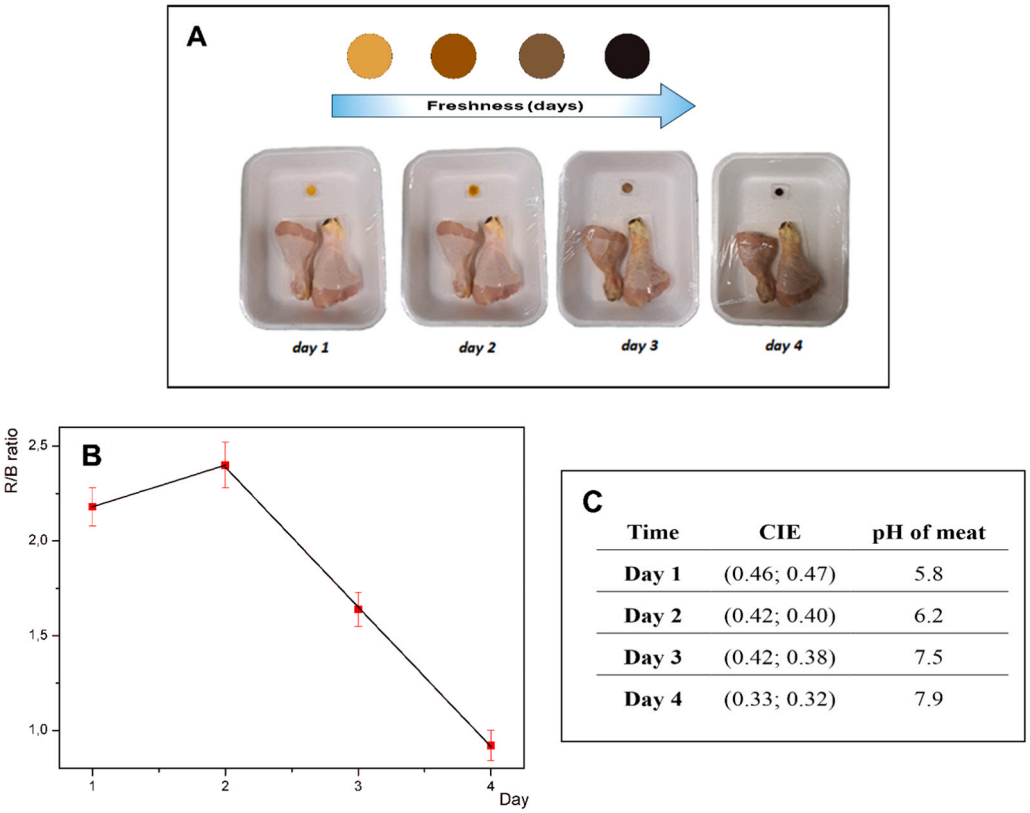


**Fig. 9.** (A): Visual monitoring of packaged chicken freshness at 25 °C for 4 days (photograph in natural diffused and shadowed light) and colour evolution of T-gel samples as indicators of freshness. (B): Corresponding R/B colour parameters as a function of time. (C): CIE values and pH measured by pHmeter on the chicken meat at every day.

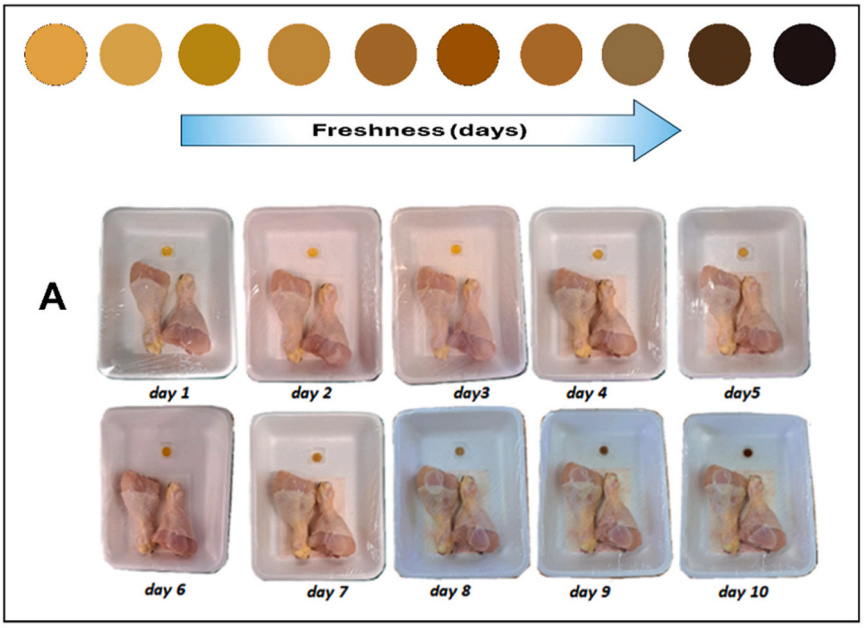


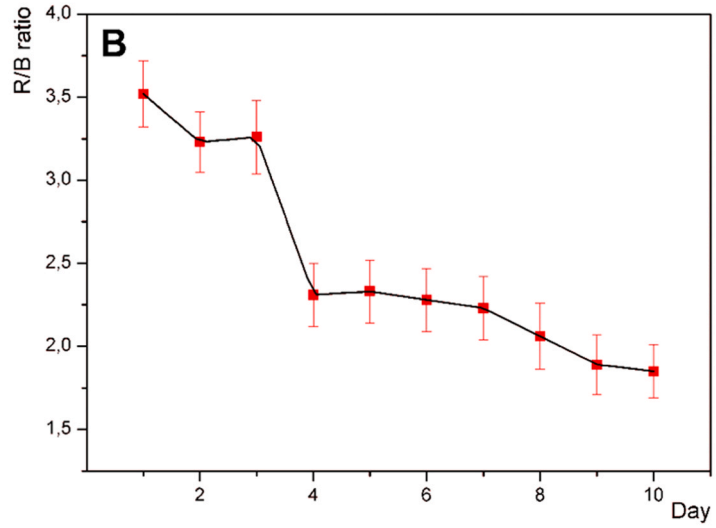


C

| Time | CIE | pH of meat | Time | CIE | pH of meat |
|---|---|---|---|---|---|
| Day 1 | (0.44; 0.45) | 5.8 | Day 6 | (0.42; 0.40) | 6.8 |
| Day 2 | (0.44; 0.44) | 5.8 | Day 7 | (0.42; 0.39) | 7.5 |
| Day 3 | (0.44; 0.43) | 5.9 | Day 8 | (0.40; 0.34) | 7.7 |
| Day 4 | (0.42; 0.41) | 5.9 | Day 9 | (0.34; 0.31) | 7.8 |
| Day 5 | (0.42; 0.41) | 6 | Day 10 | (0.33; 0.31) | 7.8 |

**Fig. 10.** (A): Visual monitoring of packaged chicken freshness at 4 °C for 10 days (photograph in natural diffused and shadowed light) and colour evolution of T-gel samples as indicators of freshness. (B): Corresponding R/B colour parameters as a function of time. (C): CIE values and pH measured by pHmeter on the chicken meat at every day.

advanced stage of deterioration (Troy & Kerry, 2010). As a product of the meat supply chain, the chemical compositional of chicken changes during storage resulting in the production of TVB-Ns as biomarkers of protein and amine degradation. TVB-Ns gradually produced during spoilage mainly consist of $NH_3$ and volatile amines, able to change the pH value in the package headspace (Chen et al., 2019). The major critical issues of the spoilage colorimetric indicators concern sensitivity, durability, ease of use, and ease of naked-eye perception. Storage temperature is a determining factor. In many cases, low storage temperature is a limitation of the sensing tool, due to the low number of TVB-Ns in the package headspace (Sutthasupa et al., 2021).

In our research, T-gel has proven to be a sensitive device capable of gradually changing color even at low temperatures. Its colorimetric response was evaluated both in accelerated spoiling conditions (25 °C) and at refrigerated temperature (4 °C). In both experiments, T-gel samples were used as an intelligent packaging, placed in a PE capsule

separated from the food sample consisting of two chicken thighs (about 300 g) packaged in a PS tray (approximately 20×10 cm). The chicken thighs were used as marketed (no need to chop them to increase the surface area).

The colour monitoring was carried out from day 1 to day 4 at 25 °C (Fig. 9), and from day 1 to day 10 at 4 °C (Fig. 10). The colour change of the hydrogel sensor was assumed to be associated with the increase in TVB-N and pH. The initial colour of T-gel is the yellow-orange colour corresponding to pH=7; in both monitoring conditions, the colour changes were clearly naked-eye perceivable from the beginning to the end of the experiment.

In the experiments carried out at 25 °C, the chicken samples can be considered from fresh to medium-fresh in days 1 and 2, and R/B parameter falls in the yellow-red zone of the colour diagram (Katiyo et al., 2020). From day 3 the product starts spoiling and the R/B parameter slumps in the magenta-violet zone. In day 4 the product is clearly "spoiled" as indicated by the dark violet color of T-gel (Fig. 9 A). The corresponding R/B colour parameters as a function of time and the CIE values are reported in Fig. 9 B and Fig. 9 C, respectively.

In the experiments carried out at 4 °C for 10 days, the colour parameters remain quite constant for days 1–3. In days 4–5 they gradually turn to a lightly darker orange colour, still falling in the yellow-red zone of the CIE diagram. In days 6–7 the orange enhances (at the limits of the yellow zone in the CIE diagram). From day 8 to day 10 the sample turns from spoiling to spoiled and the color turns to magenta-violet and finally dark violet (Fig. 10 A), indicative of the neat alkaline pH value of the gaseous phase. The corresponding R/B colour parameters as a function of time and the CIE values are reported in Fig. 10 B and Fig. 10 C, respectively. As expected, in the correct storage conditions (4 °C) the color of the indicator does not vary continuously and undergoes a sharp change starting from day 5. This indicates that the chicken meat of our experiment can be considered fresh for day 1–3, medium fresh for day 4–5, spoiling from day 6–7. Starting from day 8, the sample can be considered spoiled.

As a validation of the trials, pH of the chicken meat was determined at each stage by the pHmeter (see Sect. 2.8). As documented by relevant literature (Kim et al., 2022) changes are expected both in the TVB-N production and in the pH value of the chicken meat. The trend of the pH parameter due to the spoilage degree in the chicken meat was correlated with the CIE colour parameter of the indicator in accelerated conditions (Fig. 9 C) and in refrigerated conditions (Fig. 10 C). In both cases, the initial pH value (pH of meat = 5.8) fits with the literature indication (pH=5.7–6) for the fresh product. Then the pH of the chicken meat increases, due to proteolysis.

In the tests at 25 °C (Fig. 9 C) the trend is quick and clear. On the second day at 25 °C the pH reached the value of 6.2. The third day the sample starts spoiling, and pH was 7.5. Finally, the fourth day pH of the spoiled sample is 7.8, according with literature prevision (Chen et al., 2019). The pH value of the chicken meat at refrigerated conditions does not vary continuously (Fig. 10 C). During days 1–3 pH varies very little, the increase is most noticeable between days 4–5 and 6–7. Finally, the increase in pH is sharp between day 8 and day 10. Aside from the naked-eye test, T-gel appears to be an effective smart indicator of chicken shelf life when correlated to the appropriate calibration curve by a smartphone app.

## 4. Conclusions

A responsive soft matter sensor was obtained from a novel pH-sensitive dye and an agar matrix. The dye shows high chemical stability, colorimetric variation over a wide pH range (2−12) and high color intensity. The detection tool called T-gel was obtained by co-gelling the dye at a low percentage in agar during the thermal gelation step. The gel samples show excellent water retention capability (SR is around 3900 g/g when reached the equilibrium swelling) and good compressive strength (20 % compression under 120 KPa before the breaking). T-gel provides a colorimetric response according to different linear trends at acid and alkaline pH conditions. The colorimetric pattern was monitored in water as a function of pH and in the vapor phase as a function of time. Serving as a versatile mini-laboratory, T-gel tablets were used for colorimetric monitoring of freshness of milk samples and spoilage of chicken samples, at different times (up to 10 days for chicken samples) and temperatures (4 °C or 25 °C). The ease of obtaining, the wide spectrum of intense colors, the response speed, the longevity, the versatility are the strong point of the sensor. By correlating a colorimetric app with calibration curve management software, T-gel could be a smart tool for the consumer to monitor food shelf life via a smartphone device.

## CRediT authorship contribution statement

**Ludovica Milzi:** Investigation, Data curation. **Rosita Diana:** Writing – review & editing, Writing – original draft, Visualization, Validation, Methodology, Investigation, Formal analysis, Data curation, Conceptualization. **Pellegrino Musto:** Investigation, Data curation. **Anna Maiello:** Investigation, Data curation. **Francesco Silvio Gentile:** Investigation, Formal analysis. **Marianna Pannico:** Investigation, Data curation. **Barbara Panunzi:** Writing – review & editing, Writing – original draft, Visualization, Validation, Supervision, Resources, Project administration.

## Declaration of Competing Interest

The authors declare the following financial interests/personal relationships which may be considered as potential competing interests: Barbara Panunzi reports financial support was provided by Ministry of Education University and Research.

## Data availability

No data was used for the research described in the article.

## Acknowledgments

None

## Appendix A. Supporting information

Supplementary data associated with this article can be found in the online version at doi:10.1016/j.jfca.2024.106667.

## References

Abbas, A.A., Dawood, K.M., 2023. Anticancer therapeutic potential of benzofuran scaffolds. RSC Adv. *13* (16), 11096–11120. https://doi.org/10.1039/D3RA01383A.

Augst, A.D., Kong, H.J., Mooney, D.J., 2006. Alginate hydrogels as biomaterials. Macromol. Biosci. *6* (8), 623–633. https://doi.org/10.1002/mabi.200600069.

Banerjee, S., Bhattacharya, S., 2011. Compressive textural attributes, opacity and syneresis of gels prepared from gellan, agar and their mixtures. J. Food Eng. *102* (3), 287–292. https://doi.org/10.1016/j.jfoodeng.2010.08.025.

Baroutaji, A., Wilberforce, T., Ramadan, M., Olabi, A.G., 2019. Comprehensive investigation on hydrogen and fuel cell technology in the aviation and aerospace sectors. Renew. Sustain. Energy Rev. *106*, 31–40. https://doi.org/10.1016/j.rser.2019.02.022.

Baston, O.T., Stroia, I., Moise, A.L., Barna, D., O, 2008. Refrigerated chicken meat freshness. Correlation between easily hydrolisable nitrogen, pH value and biogenic amines contents. Ann. Univ. Dunarea De. Jos Galati. Fascicle VI - Food Technol. Vol 32 (2008).

Becke, A.D., 1992. Densityâ??functional thermochemistry. I. The effect of the exchangeâ??only gradient correction. J. Chem. Phys. *96* (3), 2155–2160. https://doi.org/10.1063/1.462066.

Bekhit, A.E.-D.A., Holman, B.W.B., Giteru, S.G., Hopkins, D.L., 2021. Total volatile basic nitrogen (TVB-N) and its role in meat spoilage: A review. Trends Food Sci. Technol. *109*, 280–302. https://doi.org/10.1016/j.tifs.2021.01.006.

Bellamy, L.J. (1975). *The Infrared Spectra of Complex Molecules*. London.

Bertasa, M., Poli, T., Riedo, C., Di Tullio, V., Capitani, D., Proietti, N., Scalarone, D., 2018. A study of non-bounded/bounded water and water mobility in different agar gels. Microchem. J. *139*, 306–314. https://doi.org/10.1016/j.microc.2018.03.016.

Borbone, F., Caruso, U., Diana, R., Panunzi, B., Roviello, A., Tingoli, M., Tuzi, A., 2009. Second order nonlinear optical networks with excellent poling stability from a new trifunctional thiophene based chromophore. Org. Electron. *10* (1), 53–60. https://doi.org/10.1016/j.orgel.2008.10.004.

Chambon, F., Winter, H.H., 1987. Linear Viscoelasticity at the Gel Point of a Crosslinking PDMS with Imbalanced Stoichiometry. J. Rheol. *31* (8), 683–697. https://doi.org/10.1122/1.549955.

Chaudhary, J., Thakur, S., Sharma, M., Gupta, V.K., Thakur, V.K., 2020. Development of biodegradable agar-agar/gelatin-based superabsorbent hydrogel as an efficient moisture-retaining agent. Biomolecules *10* (6 C7 - 939), 1–13. https://doi.org/10.3390/biom10060939.

Chen, H.-z, Zhang, M., Bhandari, B., Yang, C.-h, 2019. Development of a novel colorimetric food package label for monitoring lean pork freshness. Lwt *99*, 43–49. https://doi.org/10.1016/j.lwt.2018.09.048.

Diana, R., Caruso, U., Di Costanzo, L., Bakayoko, G., Panunzi, B., 2020. A novel DR/NIR T-shaped aiegen: Synthesis and x-ray crystal structure study. Crystals *10* (4). https://doi.org/10.3390/cryst10040269.

Diana, R., Caruso, U., Di Costanzo, L., Gentile, F.S., Panunzi, B., 2021. Colorimetric recognition of multiple first-row transition metals: A single water-soluble chemosensor in acidic and basic conditions. Dyes Pigments *184*, 108832. https://doi.org/10.1016/j.dyepig.2020.108832.

Diana, R., Caruso, U., Piotto, S., Concilio, S., Shikler, R., Panunzi, B., 2020. Spectroscopic behaviour of two novel azobenzene fluorescent dyes and their polymeric blends. Molecules *25* (6). https://doi.org/10.3390/molecules25061368.

Diana, R., Panunzi, B., Concilio, S., Marrafino, F., Shikler, R., Caruso, T., Caruso, U., 2019. The effect of bulky substituents on two π-conjugated mesogenic fluorophores. Their organic polymers and zinc-bridged luminescent networks. Polymers *11* (9). https://doi.org/10.3390/polym11091379.

Diana, R., Sessa, L., Concilio, S., Piotto, S., Di Costanzo, L., Carella, A., Panunzi, B., 2024. Experimental and Theoretical Insights into a Novel Lightfast Thiophene Azo Dye. Crystals *14* (1). https://doi.org/10.3390/cryst14010031.

Ding, N., Dong, S., Zhang, Y., Lu, D., Lin, J., Zhao, Q., Shi, X., 2022. Portable silver-doped prussian blue nanoparticle hydrogels for colorimetric and photothermal monitoring of shrimp and fish freshness. Sens. Actuators B: Chem. *363*, 131811 https://doi.org/10.1016/j.snb.2022.131811.

Fernández, E., López, D., Mijangos, C., Duskova-Smrckova, M., Ilavsky, M., Dusek, K., 2008. Rheological and thermal properties of agarose aqueous solutions and hydrogels. J. Polym. Sci., Part B: Polym. Phys. *46* (3), 322–328. https://doi.org/10.1002/polb.21370.

Gentile, F.S., Salustro, S., Desmarais, J.K., Ferrari, A.M., D'Arco, P., Dovesi, R., 2018. Vibrational spectroscopy of hydrogens in diamond: A quantum mechanical treatment. Phys. Chem. Chem. Phys. *20* (17), 11930–11940. https://doi.org/10.1039/c8cp00596f.

Gentile, F.S., Salustro, S., Di Palma, G., Causà, M., D'Arco, P., Dovesi, R., 2018. Hydrogen, boron and nitrogen atoms in diamond: a quantum mechanical vibrational analysis. Theor. Chem. Acc. *137* (11) https://doi.org/10.1007/s00214-018-2375-0.

Ghollasi-Mood, F., Mohsenzadeh, M., Hoseindokht, M.R., Varidi, M., 2017. Quality changes of air-packaged chicken meat stored under different temperature conditions and mathematical modelling for predicting the microbial growth and shelf life. J. Food Saf. *37* (3 C), 7–e12331. https://doi.org/10.1111/jfs.12331.

Graham, S., Marina, P.F., Blencowe, A., 2019. Thermoresponsive polysaccharides and their thermoreversible physical hydrogel networks. Carbohydr. Polym. *207*, 143–159. https://doi.org/10.1016/j.carbpol.2018.11.053.

Grau, R., Sánchez, A.J., Girón, J., Iborra, E., Fuentes, A., Barat, J.M., 2011. Nondestructive assessment of freshness in packaged sliced chicken breasts using SW-NIR spectroscopy. Food Res. Int. *44* (1), 331–337. https://doi.org/10.1016/j.foodres.2010.10.011.

Grimme, S., Bohle, F., Hansen, A., Pracht, P., Spicher, S., Stahn, M., 2021. Efficient Quantum Chemical Calculation of Structure Ensembles and Free Energies for Nonrigid Molecules. *The Journal of Physical Chemistry*. A *125* (19), 4039–4054. https://doi.org/10.1021/acs.jpca.1c00971.

Hu, X., Zhang, X., Li, Y., Shi, J., Huang, X., Li, Z., Zou, X., 2022. Easy-to-Use Visual Sensing System for Milk Freshness, Sensitized with Acidity-Responsive N-Doped Carbon Quantum Dots. Foods *11* (13 C7 - 1855). https://doi.org/10.3390/foods11131855.

Jeon, H.J., Choe, J.H., Jung, Y., Kruk, Z.A., Lim, D.G., Jo, C., 2010. Comparison of the chemical composition, textural characteristics, and sensory properties of North and South Korean native chickens and commercial broilers. Korean J. Food Sci. Anim. Resour. *30* (2), 171–178. https://doi.org/10.5851/kosfa.2010.30.2.171.

Jia, R., Tian, W., Bai, H., Zhang, J., Wang, S., Zhang, J., 2019. Amine-responsive cellulose-based ratiometric fluorescent materials for real-time and visual detection of shrimp and crab freshness. Nat. Commun. *10* (1), 795. https://doi.org/10.1038/s41467-019-08675-3.

Katiyo, W., de Kock, H.L., Coorey, R., Buys, E.M., 2020. Sensory implications of chicken meat spoilage in relation to microbial and physicochemical characteristics during refrigerated storage. Lwt *128*, 109468. https://doi.org/10.1016/j.lwt.2020.109468.

Kim, Y.-Y., Park, S.-J., Kim, J.-S., Shin, H.-S., 2022. Development of freshness indicator for monitoring chicken breast quality and freshness during storage. Food Sci. Biotechnol. *31* (3), 377–385. https://doi.org/10.1007/s10068-022-01034-x.

Korkeala, H., Alanko, T., Mäkelä, P., Lindroth, S., 1990. Lactic acid and pH as indicators of spoilage for vacuum-packed cooked ring sausages. Int. J. Food Microbiol. *10* (3), 245–253. https://doi.org/10.1016/0168-1605(90)90072-D.

Lee, K.Y., Mooney, D.J., 2001. Hydrogels for Tissue Engineering. Chem. Rev. *101* (7), 1869–1880. https://doi.org/10.1021/cr000108x.

Lin, Q., Jiang, L., Li, X., Sang, S., Ji, H., Jin, Z., Qiu, C., 2024. Starch based fat replacers in food system: Modification, structured design, and application. Food Biosci. *59*, 104149 https://doi.org/10.1016/j.fbio.2024.104149.

Liu, X., Chen, K., Wang, J., Wang, Y., Tang, Y., Gao, X., Li, J., 2020. An on-package colorimetric sensing label based on a sol-gel matrix for fish freshness monitoring. Food Chem. *307*, 125580 https://doi.org/10.1016/j.foodchem.2019.125580.

Lu, P., Yang, Y., Liu, R., Liu, X., Ma, J., Wu, M., Wang, S., 2020. Preparation of sugarcane bagasse nanocellulose hydrogel as a colourimetric freshness indicator for intelligent food packaging. Carbohydr. Polym. *249*, 116831 https://doi.org/10.1016/j.carbpol.2020.116831.

Luo, Q., Zhang, Y., Zhou, Y., Liu, S.G., Gao, W., Shi, X., 2021. Portable functional hydrogels based on silver metallization for visual monitoring of fish freshness. Food Control *123*, 107824. https://doi.org/10.1016/j.foodcont.2020.107824.

Lv, Q., Wu, M., Shen, Y., 2019. Enhanced swelling ratio and water retention capacity for novel super-absorbent hydrogel. Colloids Surf. A: Physicochem. Eng. Asp. *583*, 123972 https://doi.org/10.1016/j.colsurfa.2019.123972.

Manouchehri, F., Nookabadi, A.S., Kadivar, M., 2020. Production routing in perishable and quality degradable supply chains. Heliyon *6* (2). https://doi.org/10.1016/j.heliyon.2020.e03376.

McCoy, C.P., Stomeo, F., Plush, S.E., Gunnlaugsson, T., 2006. Soft Matter pH Sensing: From Luminescent Lanthanide pH Switches in Solution to Sensing in Hydrogels. Chem. Mater. *18* (18), 4336–4343. https://doi.org/10.1021/cm060603v.

Mezzenga, R., Schurtenberger, P., Burbidge, A., Michel, M., 2005. Understanding foods as soft materials. Nat. Mater. *4* (10), 729–740. https://doi.org/10.1038/nmat1496.

Neese, F., 2012. The ORCA program system. Wiley Interdiscip. Rev.: Comput. Mol. Sci. *2* (1), 73–78. https://doi.org/10.1002/wcms.81.

Rochas, C., Lahaye, M., Yaphe, W., 1986. Sulfate Content of Carrageenan and Agar Determined by Infrared Spectroscopy. Bot. Mar. *29* (4), 335–340. https://doi.org/10.1515/botm.1986.29.4.335.

Roeges, N.P.G., 1995. *A Guide to the Complete Interpretation of Infrared Spectral of Organic Structures*: Wiley. Chichester.

Roy, R., Sajeev, N.R., Sharma, V., Koner, A.L., 2019. Aggregation Induced Emission Switching Based Ultrasensitive Ratiometric Detection of Biogenic Diamines Using a Perylenediimide-Based Smart Fluoroprobe. ACS Appl. Mater. Interfaces *11* (50), 47207–47217. https://doi.org/10.1021/acsami.9b14690.

Shahnaz, L., Shehnaz, H., Haider, A., 2019. Fourier transform infrared (FT-IR) spectroscopic investigations of four agarophytes from northern arabian SEA. Bangladesh J. Bot. *48* (4), 925–932. https://doi.org/10.3329/bjb.v48i4.48934.

Sun, X., Agate, S., Salem, K.S., Lucia, L., Pal, L., 2021. Hydrogel-Based Sensor Networks: Compositions, Properties, and Applications—A Review. ACS Appl. Bio Mater. *4* (1), 140–162. https://doi.org/10.1021/acsabm.0c01011.

Sutthasupa, S., Padungkit, C., Suriyong, S., 2021. Colorimetric ammonia (NH3) sensor based on an alginate-methylcellulose blend hydrogel and the potential opportunity for the development of a minced pork spoilage indicator. Food Chem. *362*, 130151 https://doi.org/10.1016/j.foodchem.2021.130151.

Tako, M., Nakamura, S., 1988. Gelation mechanism of agarose. Carbohydr. Res. *180* (2), 277–284. https://doi.org/10.1016/0008-6215(88)80084-3.

Tokita M. Fau - Hikichi, K., & Hikichi, K. Mechanical studies of sol-gel transition: Universal behavior of elastic modulus. (0556-2791 (Print)).

Troy, D.J., Kerry, J.P., 2010. Consumer perception and the role of science in the meat industry. Meat Sci. *86* (1), 214–226. https://doi.org/10.1016/j.meatsci.2010.05.009.

Van Vlierberghe, S., Dubruel, P., Schacht, E., 2011. Biopolymer-Based Hydrogels As Scaffolds for Tissue Engineering Applications: A Review. Biomacromolecules *12* (5), 1387–1408. https://doi.org/10.1021/bm200083n.

Wang, A., Shi, W., Huang, J., Yan, Y., 2016. Adaptive soft molecular self-assemblies. Soft Matter *12* (2), 337–357. https://doi.org/10.1039/C5SM02397A.

Weigend, F., 2006. Accurate Coulomb-fitting basis sets for H to Rn. Phys. Chem. Chem. Phys. *8* (9), 1057–1065. https://doi.org/10.1039/B515623H.

Weston, M., Kuchel, R.P., Ciftci, M., Boyer, C., Chandrawati, R., 2020. A polydiacetylene-based colorimetric sensor as an active use-by date indicator for milk. J. Colloid Interface Sci. *572*, 31–38. https://doi.org/10.1016/j.jcis.2020.03.040.

Ye, H., Koo, S., Beitong, Z., Ke, Y., Sheng, R., Duan, T., Kim, J.S., 2022. Real-Time Fluorescence Screening Platform for Meat Freshness. Anal. Chem. *94* (44), 15423–15432. https://doi.org/10.1021/acs.analchem.2c03326.

Zeng, L., Xiao, X., Ye, H., Ma, D., Zhou, J., 2022. Fast visual monitoring of the freshness of beef using a smart fluorescent sensor. Food Chem. *394* https://doi.org/10.1016/j.foodchem.2022.133489.

Zhang, J., Yang, Y., Zeng, L., Wang, J., 2024. A ratiometric fluorescence platform for on-site screening meat freshness. Food Chem. *436*, 137769 https://doi.org/10.1016/j.foodchem.2023.137769.

Zhou, X., Shi, Q.-H., Bai, S., Sun, Y., 2004. Dense pellicular agarose–glass beads for expanded bed application:: Fabrication and characterization for effective protein adsorption. Biochem. Eng. J. *18* (2), 81–88. https://doi.org/10.1016/S1369-703X(03)00169-4.